JCTC Journal of Chemical Theory and Computation

pubs.acs.org/JCTC Article

Nonadiabatic Dynamics of Intersystem Crossings with the Symmetrical Quasi-Classical Dynamics Method Based on the Meyer−Miller Mapping Hamiltonian

Haiyi Huang, Jiawei Peng, Zhenggang Lan, Deping Hu,* and Ya-Jun Liu*

Cite This: J. Chem. Theory Comput. 2025, 21, 4386−4396 Read Online

ACCESS | Metrics & More | Article Recommendations | Supporting Information

ABSTRACT: We extended the symmetric quasi-classical (SQC) method based on the Meyer−Miller mapping Hamiltonian (MM) to treat the nonadiabatic dynamics simulation including spin−orbit couplings (SOCs). We studied the photoinduced ultrafast excited state dynamic involving intersystem crossing (ISC) process of the $ReBr(CO)_3bpy$ molecule by performing the dynamics based on a preconstructed model Hamiltonian as well as with the on-the-fly ab initio calculations. For the model system, the dynamics results obtained with the SQC/MM method compare very well with those obtained with the ML-MCTDH method. The SQC/MM method also outperforms the widely used trajectory surface hopping (TSH) method for the system studied here. For the realistic system, we employed the quasi-diabatic propagation scheme to enable on-the-fly ab initio dynamics with the SQC/MM method. In this case, the dynamics results obtained with the SQC/MM method are very similar to those obtained with the TSH method, and both of them show great discrepancy with the model system results, which implies it is necessary to perform the full atom on-the-fly dynamics for some molecular systems. Due to the great performance of the SQC/MM method in this work, we strongly recommend using it in the study of ISC processes in the future, for both model and realistic systems. The implementation of the SQC/MM method in the on-the-fly dynamics including the SOCs also paves the way to employing the SQC/MM or other more advanced semiclassical dynamics methods based on the mapping Hamiltonian to study the ISC processes for complex realistic molecular systems.

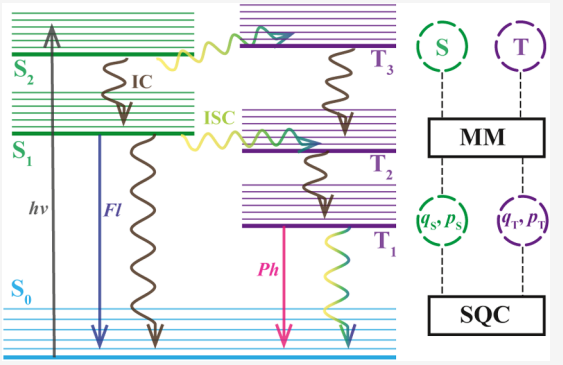

Downloaded via BEIJING NORMAL UNIV on June 6, 2025 at 02:59:58 (UTC).
See https://pubs.acs.org/sharingguidelines for options on how to legitimately share published articles.

1. INTRODUCTION

The molecular system could go to the excited states through photoexcitation, electro-excitation, or chemical excitation, then undergo a series of complex photophysical or photochemical processes.[1−4] During these processes, the molecule can transition from one state to another state with or without photo emission, namely, radiative or nonradiative transition. The nonradiative transition includes the internal conversion (IC) between electronic states with the same spin multiplicity, and the intersystem crossing (ISC) between electronic states with differing spin multiplicities. The ISC caused by the spin−orbit couplings (SOCs) play crucial roles in many processes,[5] such as the excited state dynamics of transition metal complex,[6−8] thermally activated delayed fluorescence,[9−11] and bioluminescence.[12,13]

Nonadiabatic dynamics simulation is one of the most important tools to study the ISC processes.[5,14−16] In the past decades, various nonadiabatic dynamics methods have been developed to treat the ultrafast dynamics involving ISC processes.[6,16−19] Among these methods, the exact full quantum dynamics methods,[20−22] which treat both the nuclei and electrons quantum mechanically, show high accuracy but need large computational costs. Hence, they are limited to dealing with relatively small systems. The mixed quantum-classical methods,[14] especially the trajectory surface hopping (TSH) method,[23,24] which treats the nuclei classically and the electrons quantum mechanically, can well balance the accuracy and computational efficiency and are easy to integrate with the on-the-fly dynamics. Theoretical researchers have made large efforts to implement the TSH method to treat the ISC processes.[15,16,25−28] Until now, several nonadiabatic dynamics simulation packages can support the study of the ultrafast dynamics involving ISC processes for realistic complex molecular systems with the TSH method, such as SHARC,[17,25,29] Newton-X,[28] and GTSH.[26] Based on these packages, many different kinds of important photophysical and photochemical processes involving the ISC have been investigated.[17,25−30] Although the TSH method has achieved great success in the studies of the ISC processes, it still suffers

Received: March 10, 2025
Revised: April 9, 2025
Accepted: April 10, 2025
Published: April 21, 2025

ACS Publications © 2025 American Chemical Society

from the incorrect description of the electronic coherence[31] and needs invoking *ad hoc* decoherence corrections.

Recently, the symmetric quasi-classical dynamics based on the Meyer−Miller mapping Hamiltonian (SQC/MM) method[32−34] has been developed to investigate the nonadiabatic dynamics. In the Meyer−Miller mapping model, a Hamiltonian with N discrete quantum states is mapped to a mapping Hamiltonian with N coupled harmonic oscillators. Then, the SQC/MM method can be formulated by including the zero-point energy (ZPE) in the mapping Hamiltonian and using the "bin" technique to perform the initial sampling and the final assignment of the quantum states. In the SQC/MM dynamics, the nuclei and electrons are treated in equal footing, thereby avoiding additional decoherence correction.[35] Since the SQC/MM method was put by Cotton and Miller,[33,34] they have proposed several different approaches in the implementation, such as introducing the triangle window and extending it to multiple states,[36,37] performing the dynamics in adiabatic representation and using the trajectory-adjusted electronic ZPE correction.[38] All of these efforts made the SQC/MM method a powerful tool to treat the nonadiabatic processes, and it has widely been applied to various types of ultrafast dynamics.[39−55]

Considering the SQC/MM approach has proved to be a promising tool to deal with the nonadiabatic dynamics and several previous work also demonstrated that the SQC/MM method outperforms the TSH method in some cases in the treatment of the IC processes,[44,50,56] it is natural to extend the SQC/MM method to perform the ISC dynamics. Therefore, in this work, we aim to further develop the SQC/MM method to simulate the nonadiabatic dynamics involving the ISC processes. We will validate the accuracy of the SQC/MM method by performing the dynamics for a typical model system and compare the dynamics results with those of the TSH dynamics, as well as the exact full quantum dynamics. We will also combine the SQC/MM method with the on-the-fly dynamics, and implement it in the JADE-NAMD package[57] of our group, making it available to study the nonadiabatic dynamics involving the ISC process for a realistic molecular system.

In this work, the photoinduced excited state process of a rhenium(I) complex ($ReBr(CO)_3bpy$) will be studied in both the model and realistic systems dynamics. As a typical transition metal complex, $ReBr(CO)_3bpy$ has large SOCs due to the existence of the Re atom. Cannizzo et al. showed that it will exhibit a fast ISC process after excitation to the singlet excited state and populate another two triplet metal-to-ligand charge transfer states in ∼100 fs.[58] Eng et al. constructed a spin-vibronic model Hamiltonian for the $ReBr(CO)_3bpy$ complex, based on which they further performed the multiconfiguration time-dependent Hartree (MCTDH) dynamics to investigate the ultrafast excited state dynamics processes. For convenience, the model system dynamics in our study will also be based on the Hamiltonian constructed by Eng et al.[58] In addition, we will perform the on-the-fly dynamics for a realistic $ReBr(CO)_3bpy$ complex. In this case, we can directly compare the dynamics results obtained from the model and realistic system dynamics.

2. THEORY AND METHODS

In this work, we implemented the SQC/MM method in the study of ISC processes for both model and realistic molecular systems. We compared the results with those obtained with the TSH method. Next, we give a brief introduction to the SQC/MM methods, as well as the quasi-diabatic (QD) propagation approach used here. The details of the implementation of ISC dynamics with the TSH method are provided in the Supporting Information.

2.1. Meyer-Miller Hamiltonian. A generic representation of a Hamiltonian operator for a molecular system with F electronic states can be written as

$$\hat{H} = \frac{\mathbf{P}^2}{2\mathbf{M}} + \sum_{i,j}^{F} \hat{a}_i^{\dagger} V_{ij}(\mathbf{R}) \hat{a}_j \tag{1}$$

where $\hat{a}_i^{\dagger}$ and $\hat{a}_j$ are the creation and annihilation operators, respectively. To derive the MM Hamiltonian, one way is to take the electronic degrees of freedom (DOFs) in eq 1 to be harmonic oscillators and then express the ladder operators in terms of coordinate and momentum operators as

$$\hat{a}_i^{\dagger} = \frac{1}{\sqrt{2}}(\hat{x}_i - i\hat{p}_i) \tag{2a}$$

$$\hat{a}_j = \frac{1}{\sqrt{2}}(\hat{x}_j + i\hat{p}_j) \tag{2b}$$

Substituting eqs 2a and 2b into eq 1, we get

$$\hat{H} = \frac{\mathbf{P}^2}{2\mathbf{M}} + \sum_{i}^{F}\left(\frac{1}{2}\hat{p}_i^2 + \frac{1}{2}\hat{x}_i^2 - \frac{1}{2}\right)V_{ii}(\mathbf{R}) + \frac{1}{2}\sum_{i\neq j}^{F}(\hat{p}_i\hat{p}_j + \hat{x}_i\hat{x}_j + i\hat{x}_i\hat{p}_j - i\hat{p}_i\hat{x}_j)V_{ij}(\mathbf{R}) \tag{3}$$

Note that the imaginal terms for the off-diagonal part above were dropped in most of the previous studies,[34,36,38] since the electronic Hamilton matrix elements $H_{ij}(\mathbf{R})$ of them are real and the imaginal terms cancel out. However, in this work on the ISC dynamics, the SOC terms, which appear in $H_{ij}(\mathbf{R})$, are complex, so we still keep the imaginal terms ($i\hat{x}_i\hat{p}_j$ and $i\hat{p}_i\hat{x}_j$) in eq 3. Then, the classical MM Hamiltonian can be obtained by replacing all the quantum operators with their classical counterparts

$$H = \frac{\mathbf{P}^2}{2\mathbf{M}} + \sum_{i}^{F}\left(\frac{1}{2}p_i^2 + \frac{1}{2}x_i^2 - \gamma_i\right)V_{ii}(\mathbf{R}) + \frac{1}{2}\sum_{i\neq j}^{F}(x_ix_j + p_ip_j)\mathbf{Re}[V_{ij}(\mathbf{R})] - \sum_{i\neq j}^{F} x_ip_j\mathbf{Im}[V_{ij}(\mathbf{R})] \tag{4}$$

where γ_i is viewed as a parameter,[39] which specifies the ZPE of the mapping oscillators[39,59−61] and is different for each state in the γ-adjusted SQC/MM approach[36,38] used in this work. For convenience, we separated the real and imaginary parts of the electronic Hamiltonian in the above equations.

After we get the classical Hamiltonian for the whole system, the equations of motion for nuclei and electrons are generated based on the Hamilton's equations of motion

$$\dot{p}_i = -x_iV_{ii}(\mathbf{R}) - \sum_{i\neq j}^{F} x_j\mathbf{Re}[V_{ij}(\mathbf{R})] + \sum_{i\neq j}^{F} p_j\mathbf{Im}[V_{ij}(\mathbf{R})] \tag{5a}$$

https://doi.org/10.1021/acs.jctc.5c00397
J. Chem. Theory Comput. 2025, 21, 4386−4396

$$\dot{x}_i = p_i V_{ii}(\mathbf{R}) + \sum_{i\neq j}^{F} p_j \mathbf{Re}[V_{ij}(\mathbf{R})] + \sum_{i\neq j}^{F} x_j \mathbf{Im}[V_{ij}(\mathbf{R})] \tag{5b}$$

$$\dot{\mathbf{P}} = -\sum_{i}^{F}\left(\frac{1}{2}x_i^2 + \frac{1}{2}p_i^2 - \gamma_i\right)\frac{\partial V_{ii}(\mathbf{R})}{\partial \mathbf{R}} - \frac{1}{2}\sum_{i\neq j}^{F}(x_i x_j + p_i p_j)\mathbf{Re}\left[\frac{\partial V_{ij}(\mathbf{R})}{\partial \mathbf{R}}\right] + \sum_{i\neq j}^{F} x_i p_j \mathbf{Im}\left[\frac{\partial V_{ij}(\mathbf{R})}{\partial \mathbf{R}}\right] \tag{5c}$$

$$\dot{\mathbf{R}} = \frac{\mathbf{P}}{\mathbf{M}} \tag{5d}$$

where $\frac{\partial V_{ij}(\mathbf{R})}{\partial \mathbf{R}}$ represents the first-order derivative of the electronic Hamiltonian with respect to the nuclear coordinates. As mentioned before, the imaginary part of the electronic Hamiltonian comes from the SOCs between the singlet and triplet states. However, the first-order derivatives of the SOCs are not available with the TDDFT method that we used in this work. Considering the change of SOCs with respect to the nuclear coordinates is small, we neglected these terms in the calculation of $\frac{\partial V_{ij}(\mathbf{R})}{\partial \mathbf{R}}$, which means we dropped term $\sum_{i\neq j}^{F} x_i p_j \mathbf{Im}\left[\frac{\partial V_{ij}(\mathbf{R})}{\partial \mathbf{R}}\right]$ in eq 5c. This approximation was also applied in previous on-the-fly ISC dynamics with the TSH method.[17,25,29] As a consequence, the total energy of the system is not conserved during the dynamics since we neglect one term in the calculation of the nuclear forces.

2.2. Window Functions and Initial Sampling. In the SQC/MM dynamics, the "window functions" were used for both the initial sampling of the electronic DOFs and determination of the final electronic states. In this work, we used the triangle window proposed by Cotton and Miller,[36,38] which was proved to perform best among all the window functions.

The triangle window is expressed as

$$W_i(\boldsymbol{\varepsilon} = \varepsilon_1, \ldots \varepsilon_i, \ldots \varepsilon_f) = w_1(\varepsilon_i)\prod_{i\neq j}^{F} w_0(\varepsilon_i, \varepsilon_j) \tag{6}$$

where

$$\varepsilon_i = \frac{1}{2}x_i^2 + \frac{1}{2}p_i^2 \tag{7}$$

is the action variable for state $|i\rangle$. The window functions are defined as

$$w_1(\varepsilon_i) = \begin{cases} (2-\varepsilon_i)^{2-F}, & 1 < \varepsilon_i < 2 \\ 0 & \text{else} \end{cases} \tag{8}$$

and

$$w_0(\varepsilon_i, \varepsilon_j) = \begin{cases} 1, & \varepsilon_j < 2 - \varepsilon_i \\ 0, & \text{else} \end{cases} \tag{9}$$

and trajectories are assigned to state i if $W_i = 1$ at any moment during the dynamics.

To perform the initial sampling, we first sampled the initial action variable ε_i^0 according to the window function (eq 6). Then, the initial mapping variables x_i^0 and p_i^0 are sampled as follows

$$x_i^0 = \sqrt{2\varepsilon_i^0}\cos\theta \tag{10a}$$

$$p_i^0 = -\sqrt{2\varepsilon_i^0}\sin\theta \tag{10b}$$

Here, the angles θ are uniformly sampled from 0 to 2π. At last, the γ_i is chosen to satisfy

$$\gamma_i = \varepsilon_i^0 - \delta_{ij} \tag{11}$$

2.3. Quasi-Diabatic Propagation Approach. To perform on-the-fly dynamics with the SQC/MM approach, the QD propagation approach was used in this work. The QD method can connect the SQC/MM approach, which was originally formulated in the diabatic representation, with the adiabatic electronic structure calculations, and achieved great successes in previous work.[49,56,62,63] Next, I briefly introduce this method.

For one molecule at nuclear configuration $\mathbf{R}$, it is convenient to obtain the adiabatic states under the molecular Coulomb Hamiltonian $\{|\Phi_i(\mathbf{R})\rangle\}$ and corresponding energies $\{E_i(\mathbf{R})\}$ with the electronic structure calculations. The QD scheme directly uses the adiabatic states associated with a reference geometry as the local diabatic states during a short-time quantum propagation, and dynamically updates the definition of the QD states along the time-dependent nuclear trajectory. Between two consecutive nuclear geometries in the time evolution, $\mathbf{R}(t_0)$ and $\mathbf{R}(t_1)$, one can use the adiabatic states at $\mathbf{R}(t_0)$ as a QD basis to propagate the electronic subsystem to the next nuclear geometry $\mathbf{R}(t_1)$. In particular, the basis

$$\{|\Phi_i(\mathbf{R}_0)\rangle\} \equiv \{|\Phi_i(\mathbf{R}(t_0))\rangle\}, \text{ for } t \in [t_0, t_1] \tag{12}$$

is taken and used to represent the potential energy $\hat{V}(\hat{\mathbf{r}}, \mathbf{R})$ at all electronic time steps between $\mathbf{R}(t_0)$ and $\mathbf{R}(t_1)$,

$$V_{ij}(\mathbf{R}(t)) = \langle\Phi_i(\mathbf{R}_0)|\hat{V}(\mathbf{R}(t))|\Phi_j(\mathbf{R}_0)\rangle \tag{13}$$

At each electronic time step, an interpolation (between nuclear geometries $\mathbf{R}(t_0)$ and $\mathbf{R}(t_1)$) of the potential energy operator is obtained in the basis of $\mathbf{R}(t_0)$, implying that all interpolated steps produce an off-diagonal electronic matrix in this basis. Most importantly, note that in this QD basis, the derivative couplings vanish by definition.

The linear interpolation between $V_{ij}(\mathbf{R}(t_0))$ and $V_{ij}(\mathbf{R}(t_1))$ is computed as

$$V_{ij}(\mathbf{R}(t)) = V_{ij}(\mathbf{R}_0) + \frac{(t-t_0)}{(t_1-t_0)}[V_{ij}(\mathbf{R}(t_1)) - V_{ij}(\mathbf{R}_0)] \tag{14}$$

where $V_{ij}(\mathbf{R}_0) = \langle\Phi_i(\mathbf{R}_0)|\hat{V}(\mathbf{R}(t_0))|\Phi_j(\mathbf{R}_0)\rangle$. The matrix elements $V_{ij}(\mathbf{R}(t_1))$ are computed as follows:

$$V_{ij}(\mathbf{R}(t_1)) = \sum_{kl} S_{ik} V_{kl}(\mathbf{R}(t_1)) S_{jl}^{\dagger} \tag{15}$$

where $V_{kl}(\mathbf{R}(t_1)) = \langle\Phi_k(\mathbf{R}(t_1))|\hat{V}(\mathbf{R}(t_1))|\Phi_l(\mathbf{R}(t_1))\rangle$. Note that $V_{ij}(\mathbf{R}_0)$ and $V_{kl}(\mathbf{R}(t_1))$ are not diagonalized due to the existence of the SOC terms. The overlap matrix between two adiabatic electronic states (at two different nuclear geometries) is $S_{ik} = \langle\Phi_i(\mathbf{R}_0)|\Phi_k(\mathbf{R}(t_1))\rangle$ and $S_{jl}^{\dagger} = \langle\Phi_l(\mathbf{R}(t_1))|\Phi_j(\mathbf{R}_0)\rangle$.

https://doi.org/10.1021/acs.jctc.5c00397
J. Chem. Theory Comput. 2025, 21, 4386−4396

The nuclear gradients $\nabla V_{ij}(\mathbf{R}(t_1)) \equiv \partial V_{ij}(\mathbf{R}(t_1))/\partial \mathbf{R}$ are evaluated as

$$\begin{aligned}\nabla V_{ij}(\mathbf{R}(t_1)) &= \nabla\langle\Phi_i(\mathbf{R}_0)|\hat{V}(\mathbf{R}(t_1))|\Phi_j(\mathbf{R}_0)\rangle \\ &=\langle\Phi_i(\mathbf{R}_0)|\nabla\hat{V}(\mathbf{R}(t_1))|\Phi_j(\mathbf{R}_0)\rangle \\ &=\sum_{kl} S_{ik}\langle\Phi_k(\mathbf{R}(t_1))|\nabla\hat{V}(\mathbf{R}(t_1))|\Phi_l(\mathbf{R}(t_1))\rangle S_{jl}^{\dagger}\end{aligned} \tag{16}$$

Once the electronic DOFs are propagated to time t_1, we adopt a new basis composed of the adiabatic states at the $\mathbf{R}(t_1)$ geometry, $\{|\Phi_j(\mathbf{R}(t_1))\rangle\}$. At this time, all quantities including the Hamiltonian matrix and the mapping variables are transformed from $\{|\Phi_i(\mathbf{R}_0)\rangle\}$ to $\{|\Phi_j(\mathbf{R}(t_1))\rangle\}$ basis using the relation

$$|\Phi_j(\mathbf{R}(t_1))\rangle = \sum_i \langle\Phi_i(\mathbf{R}(t_0))|\Phi_j(\mathbf{R}(t_1))\rangle|\Phi_i(\mathbf{R}(t_0))\rangle \tag{17}$$

After that, we propagate the system from $\mathbf{R}(t_1)$ and $\mathbf{R}(t_2)$ using the same strategy as above and repeat the short-time propagation until the end of the dynamics.

3. COMPUTATIONAL DETAILS

In this work, we investigated the performance of the SQC/MM method in the study of the ISC process of the $ReBr(CO)_3bpy$ molecule in both model and realistic forms. Next, I will introduce the details of the model Hamiltonian used in the model system dynamics and the electronic structure calculations in the on-the-fly dynamics process.

3.1. Model Hamiltonian. We used the same model constructed by Eng et al. in their work on spin-vibronic quantum dynamics of the $ReBr(CO)_3bpy$ molecule.[6] We will briefly introduce the model Hamiltonian used here, and the details can be found in the original paper.[6] The total model Hamiltonian is expressed as

$$\mathbf{H} = T_N\mathbf{1} + \mathbf{H}^{el} \tag{18}$$

where T_N is the nuclear kinetic energy, $\mathbf{1}$ is the identical matrix, and $\mathbf{H}^{el}$ is the electronic Hamiltonian which depends on the nuclear coordinates.

Then, the effective Hamiltonian is written as

$$\mathbf{H} = (T_N + V_0)\mathbf{1} + \mathbf{W} \tag{19}$$

where V_0 is the potential energy which is harmonic with vibrational frequencies. $\mathbf{W}$ is defined as

$$\mathbf{W} = \begin{Bmatrix} \mathbf{W}^{T_1,T_1} & \mathbf{W}^{T_1,T_2} & 0 & \mathbf{W}^{T_1,S_2} & 0 \\ \mathbf{W}^{*T_1,T_2} & \mathbf{W}^{T_2,T_2} & \mathbf{W}^{T_2,S_1} & 0 & \mathbf{W}^{T_2,T_3} \\ 0 & \mathbf{W}^{*T_2,S_1} & \mathbf{W}^{S_1,S_1} & \mathbf{W}^{S_1,S_2} & \mathbf{W}^{S_2,T_3} \\ \mathbf{W}^{*T_1,S_2} & 0 & \mathbf{W}^{*}S_1,\ S_2 & \mathbf{W}^{S_2,S_2} & \mathbf{W}^{S_2,T_3} \\ 0 & \mathbf{W}^{*T_2,T_3} & 0 & \mathbf{W}^{*S_2,T_3} & \mathbf{W}^{T_3,T_3} \end{Bmatrix} \tag{20}$$

where

$$\mathbf{W}^{n,n} = E_n + \sum_{i\in a'} \lambda_i^{\,n} Q_i,\ \mathbf{W}^{S_1,S_2} = \sum_{j\in a''} \lambda_j^{S_1,S_2} Q_j$$

$$\mathbf{W}^{S_2,T_3} = \begin{pmatrix} \eta^{*}_{S_2,T_3} & 0 & \eta_{S_2,T_3} \end{pmatrix},\ \mathbf{W}^{T_n,S_m} = \begin{pmatrix} \eta_{S_m,T_n} \\ 0 \\ \eta^{*}_{S_m,T_n} \end{pmatrix}$$

$$\mathbf{W}^{T_1,T_2} = \begin{Bmatrix} \sum_{j\in a''} \lambda_j^{T_1,T_2} Q_j & \eta_{T_1,T_2} & 0 \\ -\eta^{*}_{T_1,T_2} & \sum_{j\in a''} \lambda_j^{T_1,T_2} Q_j & \eta_{T_1,T_2} \\ 0 & -\eta^{*}_{T_1,T_2} & \sum_{j\in a''} \lambda_j^{T_1,T_2} Q_j \end{Bmatrix}$$

and

$$\mathbf{W}^{T_2,T_3} = \begin{Bmatrix} 0 & \eta_{T_2,T_3} & 0 \\ -\eta^{*}_{T_2,T_3} & 0 & \eta_{T_2,T_3} \\ 0 & -\eta^{*}_{T_2,T_3} & 0 \end{Bmatrix}$$

Here, all parameters used in the model Hamiltonian are defined in previous work[6] and are presented in the Supporting Information for convenience. The model system consists of two excited singlet states (S_1 and S_2), three lowest-energy triplet states (T_1, T_2, and T_3), and six nuclear vibrational modes. The motion patterns of the nuclear modes are shown in Figure 1.

The model constructed above was used in the multilayer MCTDH (ML-MCTDH),[64,65] TSH and SQC/MM dynamics. A brief introduction to the ML-MCTDH method and the related computational details are presented in the Supporting Information. For the SQC/MM and TSH approaches, the

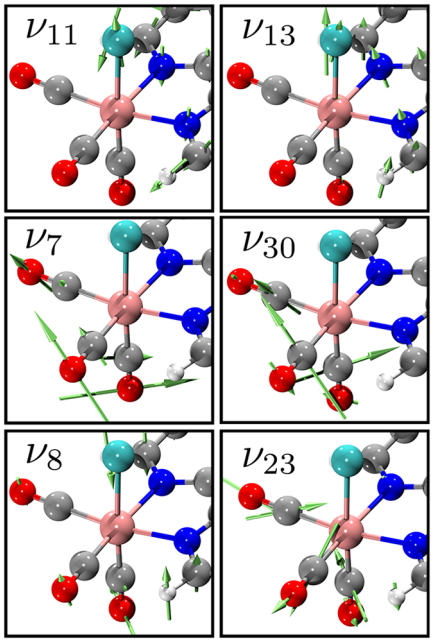

Figure 1. Chosen vibrational DOFs in the model system of the $ReBr(CO)_3bpy$ molecule. Green arrows denote the motion vectors. ν_{11} and ν_{13} indicate the stretching motion of the Re−Br bond; ν_7 and ν_{30} indicate the symmetric motion of the carbonyl groups; and ν_8 and ν_{23} indicate the asymmetric motion of the carbonyl groups.

https://doi.org/10.1021/acs.jctc.5c00397
J. Chem. Theory Comput. 2025, 21, 4386−4396

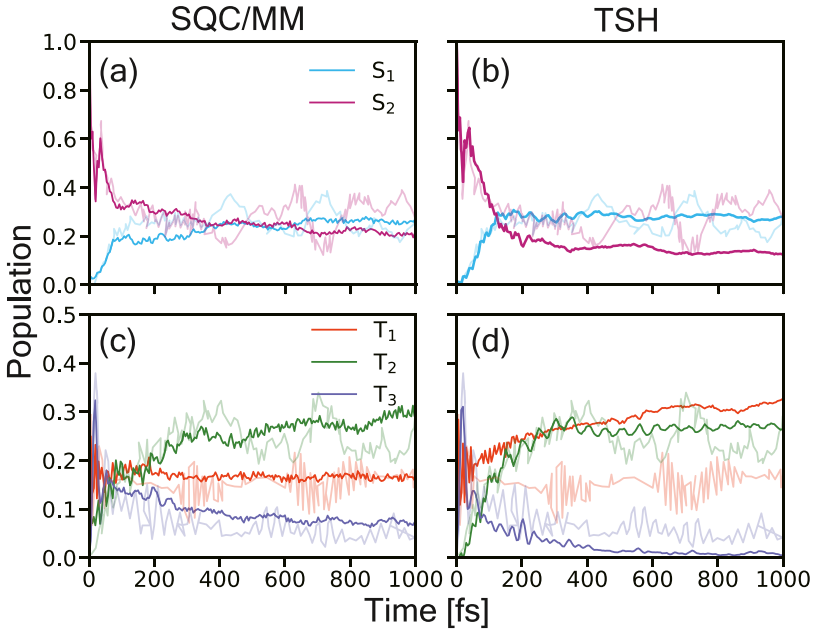

Figure 2. Time-dependent population of the spin-diabatic states for the $ReBr(CO)_3bpy$ model system, as propagated by the SQC/MM (left) and TSH (right) methods. The dynamics results generated by the ML-MCTDH method are shown in translucent colors. The singlet and triplet state populations are presented at the top and bottom, respectively.

nuclear time steps and electronic time steps were set as 0.5 and 0.005 fs, respectively. The total simulation time was 1000 fs. A number of 10000 trajectories were used to converge the dynamics results, see the convergence test in Figure S1 in the Supporting Information.

3.2. On-the-Fly Dynamics. The on-the-fly nonadiabatic dynamics were performed for the $ReBr(CO)_3bpy$ molecular system with the TSH and SQC/MM approaches. Initially, $ReBr(CO)_3bpy$ was optimized at the ground state, with subsequent frequency evaluations performed at the DFT level using the PBE0 functional[66,67] with a mixed basis set (LANL2DZ basis set for the Re atom with LANL2DZ pseudopotential[68] and 6-31G basis set[69] for other atoms). Grimme's D3BJ dispersion[70] was employed to correct dispersion effects. An implicit solvent model was adopted, with acetonitrile (ϵ = 35.688) as the solvent using the conductor-like polarizable continuum (C-PCM) model formalism.[71,72] The TDDFT method was used to calculate the excited state energies, while the Tamm-Dancoff approximation was applied. Both the optimization and frequency analysis were performed using the Gaussian 16 package,[73] while the Wigner sampling was executed via JADE-NAMD package.[57]

Then, the Wigner sampling[74] was conducted based on the optimized structure and corresponding frequencies, generating 200 initial coordinates and velocities at 300 K. The energies and gradients of all states, nonadiabatic couplings, between states with the same multiplicities, and SOCs between states with differing multiplicities were computed at each nuclear step using the Q-CHEM 5.1 package.[75] The electronic structure calculations level including the solvent model used in the dynamics process is the same as the initial sampling process, and also the same as those to construct the model Hamiltonian.[6]

Population estimation was achieved by averaging over 200 trajectories for both TSH and SQC/MM dynamics. According to the ML-MCTDH population data, the populations of each electronic state stabilize nearly after 500 fs. So the simulation duration for both TSH and SQC/MM was limited to 500 fs, with a nuclear time step of 0.5 fs and an electronic time step of 0.005 fs. All the dynamics were performed with the developing version of the JADE-NAMD package.[57]

4. RESULTS AND DISCUSSION

4.1. Model System Dynamics. Figure 2 presents the time-dependent spin-diabatic state populations in the nonadiabatic dynamics simulation of the $ReBr(CO)_3bpy$ model system by using the SQC/MM, TSH, and ML-MCTDH methods.

For the ML-MCTDH dynamics, the population is presented in Figure 2 with translucent colors. The electronic populations are exactly same with those obtained with the MCTDH method in previous work.[6] The system is initially in the S_2 state. In the beginning of the dynamics, the populations of S_2 rapidly decrease from 1.0 to ~0.35 within 20 fs, mainly due to the strong SOCs between S_2 and T_1 (601.1 cm^{-1}) states, and between S_2 and T_3 (225.6 cm^{-1})[6] states. Meanwhile, the populations of T_1 and T_3 rapidly increase to 0.2−0.3, while the populations of S_1 and T_2 stay at a very low value. Next, after a fast increase to ~0.6 caused by the reverse ISC process from the T_1 and T_3, the population of S_2 gradually declined, while the population of S_1 gradually increased, mainly due to the internal conversion from S_2 to S_1. Their populations arrive at the same value (~0.25) at about 0.2 fs, and then their populations oscillate around 0.25 until the end of the dynamics. In addition, the population of T_3 gradually decreases while the population of T_2 gradually increases, mainly due to the internal conversion from T_3 to T_2. The population of T_3 arrives at about 0.05, while the population of T_2 arrives at about 0.28 at the end of the dynamics. An interesting phenomenon is that the population of T_1 oscillates around a steady value (~0.18) from 0.1 to the end of the dynamics. The rich population evolution features of this system stem from multiple IC and ISC channels during the dynamics.

https://doi.org/10.1021/acs.jctc.5c00397
J. Chem. Theory Comput. 2025, 21, 4386−4396

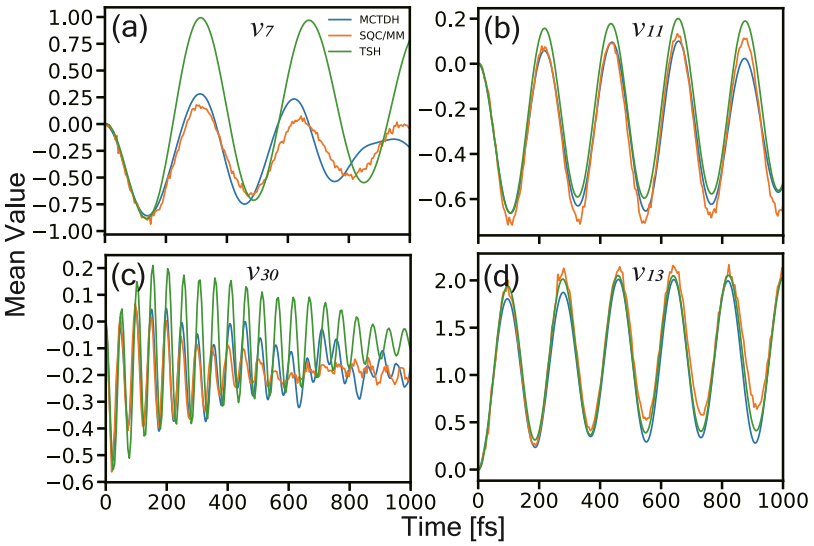

Figure 3. Time-dependent mean values of the positions for the nuclear modes: (a) ν_7; (b) ν_{11}; (c) ν_{30}; and (d) ν_{13} for the $ReBr(CO)_3bpy$ model system, as propagated by the ML-MCTDH (blue lines), SQC/MM (orange lines), and TSH (green lines) methods.

For SQC/MM, the time-dependent populations of the spin-diabatic states are presented in Figure 2(a),2(c) with opaque lines. The population dynamics compare very well with those obtained with the ML-MCTDH method. The difference between the SQC/MM and ML-MCTDH population is that the population obtained with the ML-MCTDH method shows much more drastic oscillations during the dynamics, while the population obtained with the SQC/MM oscillates slightly. Nevertheless, the SQC/MM method reproduces the dynamics features very well of the nonadiabatic for the ISC process of the model system studied in this work.

For TSH, the time-dependent populations of the spin-diabatic states are presented in Figure 2(b),2(d) with opaque lines. The population dynamics compare well with the ML-MCTDH dynamics during the first 20 fs. However, after that, the population obtained with the TSH method begins to differ from those obtained with the ML-MCTDH method. The biggest difference is the population of the T_1 state in the TSH dynamics increases a lot, while that in the ML-MCTDH dynamics remains steady until the end of the dynamics. The second difference is that the population of the S_2 state in the TSH dynamics decreases to a lower value (~0.18) than that (~0.25) in the ML-MCTDH dynamics. Besides, the populations of the T_3 state in the TSH dynamics decrease almost to zero at the end of the dynamics, while that in the ML-MCTDH dynamics is slightly higher (0.05).

Besides the electronic populations, we also checked the performance of the SQC/MM methods for the nuclear motions. Figure 3 presents the mean values of the positions for the nuclear modes (ν_7, ν_{11}, ν_{30} and ν_{13}) during dynamics propagated by the ML-MCTDH, SQC/MM, and TSH methods. Similar to the electronic populations, the nuclear evolutions obtained with the SQC/MM method compare very well with those obtained with the ML-MCTDH methods in both short- and long-time dynamics, while the results obtained with the TSH methods begin to show great discrepancy after 200 fs. The time-dependent mean values of the other two nuclear modes (ν_8 and ν_{23}) are presented in Figure S2 in the Supporting Information. Since their coordinates change slightly during the dynamics, the results will not be further discussed here.

Overall, for the electronic populations and nuclear motions of the model system, the SQC/MM method performs very well both in the short-time and long-time dynamics, while the TSH method only performs well in the short-time dynamics but fails to capture the long-time dynamics feature.

4.2. Realistic System Dynamics. After the dynamics for the model system, we also performed the on-the-fly dynamics for the realistic molecular system with the SQC/MM and TSH methods. The vertical excited energies of all states included in the nonadiabatic dynamics were presented in Table 1. We can see the calculated vertical excited energies from the ground state to S_2 were 3.07 eV, which is close to the experimental one (3.10 eV).[58] The consistency between the theoretical and experimental energies demonstrates that the electronic structure calculation levels are proper for the molecular system studied here.

Table 1. Vertical Excited Energies ΔE (eV) Calculated at the PBE0/(LANL2DZ/6-31G) Level[a]

transition pattern	theo.	exp.[58]
$S_0 \rightarrow S_1$	2.91	
$S_0 \rightarrow S_2$	3.07	3.10
$S_0 \rightarrow T_1$	2.80	
$S_0 \rightarrow T_2$	2.88	
$S_0 \rightarrow T_3$	3.35	

[a]The C-PCM solvent model was used, and the solvent is set as acetonitrile.

The time-dependent populations of the spin-diabatic state are presented in Figure 4. Figure 4(a),4(c) presents the population dynamics with the SQC/MM method. To be consistent with the model system, the realistic system is also put at the S_2 state before the dynamics. Figure 4(c) shows the population dynamics in the first 100 fs. We can see that the S_2 state undergoes ultrafast decay, with the population decreasing rapidly from 1.0 to 0.1. The population of T_1 increases rapidly from zero to 0.5, while the population of S_1 and T_2 increase slowly from zero to ~0.18. The population of T_3 first increases to ~0.12 and then decreases to ~0.02. After 100 fs, the population of S_2 and T_3 continues decreasing and arrives at

https://doi.org/10.1021/acs.jctc.5c00397
J. Chem. Theory Comput. 2025, 21, 4386−4396

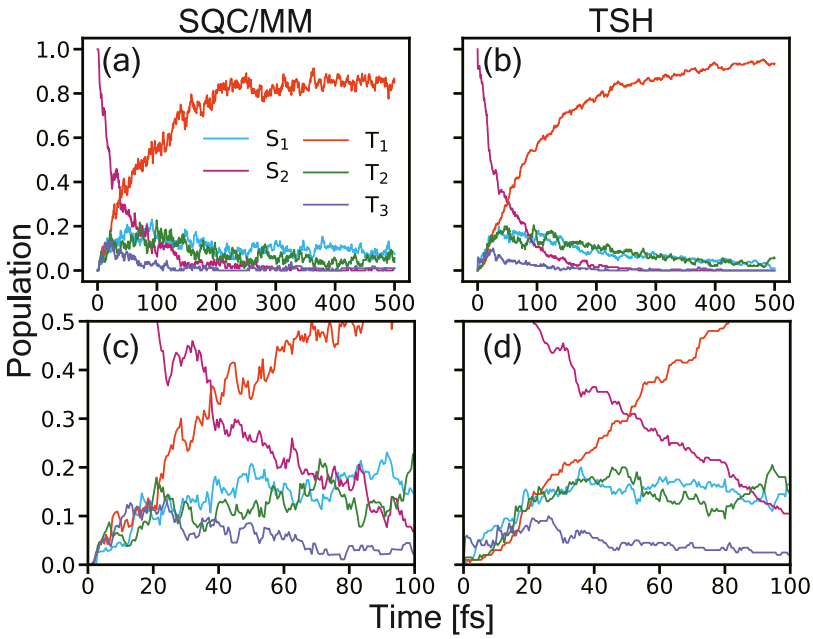

Figure 4. Time-dependent population of the spin-diabatic state in the nonadiabatic dynamics of the $ReBr(CO)_3bpy$ molecule by using the SQC/MM (left) and TSH (right) methods at the PBE0/(LANL2DZ/6−31G) level. The long-time (500 fs) and short-time (100 fs) dynamics results are shown at the top and bottom panels, respectively.

zero at ∼250 fs, then they remain zero until the end of the dynamics. The population of T_1 continues increasing and arrives at ∼0.8 at ∼250 fs, and then it oscillates around 0.8 until the end of the dynamics. The populations of S_1 and T_2 begin to decrease and arrive at ∼0.05 at the end of the dynamics.

For the TSH method, the population dynamics are presented in Figure 4(b),4(d). Compared to the population obtained by the SQC/MM method, the population of TSH dynamics is smoother, which is because we only count the trajectories inside the window to get the population in the SQC/MM dynamics. Besides, in the TSH dynamics, the population of S_2 decays a little slower and the population of T_1 increases a little slower compared to those in the SQC/MM dynamics.

When we compare the population dynamics for the realistic system (Figure 4) with those for the corresponding model system (Figure 2), they show great differences for both the SQC/MM and TSH methods. For the realistic system, most of the trajectories stay at the T_1 state at the end of the dynamics. For the model system, quite a number of trajectories also stay at other states like S_2, S_1, and T_2 at the end of the dynamics. In addition, the population obtained with the SQC/MM and TSH methods show great differences in the model system dynamics, while they are very similar to each other in the realistic system dynamics.

4.3. Difference between Model and Realistic Systems. To understand why so large discrepancies are observed between the dynamics for realistic and model systems, we plotted the distribution of energy gaps between T_1 and other states over time when the system is at the T_1 state in the dynamics with the SQC/MM method, the results are shown in Figure 5. For the model system, when the system arrives at the T_1 state, the energy gaps between T_1 and other states do not change too much and remain small values, which makes it high probability for the system to transition to other states through IC or ISC process. On the contrary, for the realistic system, the energy gaps between T_1 and other states are increasing over time and arrive at large values, which makes it low probability for the system to transition to other states. Thus, when the trajectories arrive at the T_1 state, most of them will stay at there. As a result, the T_1 state dominates the population at the end of the dynamics.

The above phenomenon could be attributed to the incompleteness of the model system. First, only six DOFs are involved in the model Hamiltonian, and other nuclear DOFs with large vibronic couplings may play important roles in the IC or ISC process in the realistic dynamics simulation. Second, the vibronic coupling and SOCs are treated as constants during the model system dynamics; they may change in realistic situations. Last, the linear vibronic coupling approximation and harmonic approximation are made in the construction of the model Hamiltonian, which may not be enough for this system, since some high-order terms, mode−model coupling, or inharmonic effects may also play key roles. Overall, it is still a challenge to develop more accurate and effective approaches to construct a proper model to mimic a realistic system. It also indicates the necessity to perform the on-the-fly ab initio dynamics to investigate the photophysical or photochemical process of some complex molecular system.

5. CONCLUSIONS

In this work, we extended the SQC/MM method to treat the nonadiabatic dynamics involving ISC process. We studied the ultrafast photoexcited decay process of the $ReBr(CO)_3bpy$ molecule system with a preconstructed linear vibronic model as well as the on-the-fly dynamics simulation. For the model system, the dynamics results obtained with the SQC/MM method compare very well with those obtained with the ML-MCTDH method. On the contrary, the TSH method can only capture the short-time dynamics features while it fails to capture the long-time dynamics features. For the realistic dynamics, the results obtained with the SQC/MM and TSH methods are very similar to each other, and both of them show

https://doi.org/10.1021/acs.jctc.5c00397
J. Chem. Theory Comput. 2025, 21, 4386−4396

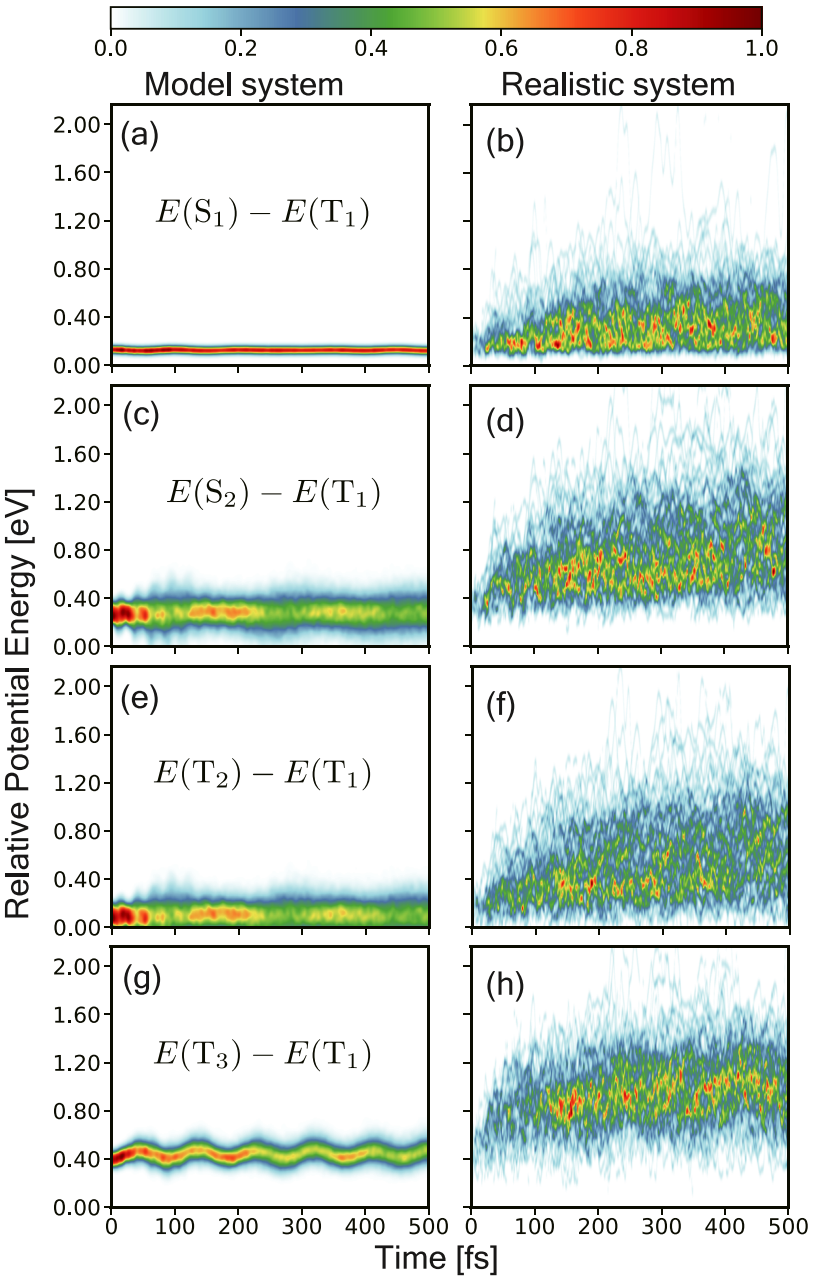

Figure 5. Distributions of the energy gaps between (a, b) S_1 and T_1, (c, d) S_2 and T_1, (e, f) T_2 and T_1, and (g, h) T_3 and T_1 over time when the system is at the T_1 state in the dynamics with the SQC/MM method. The distributions for the model system and realistic system dynamics are presented on the left and right sides, respectively.

large differences from the corresponding model system ones. We infer that the differences may be due to the incompleteness of the model Hamiltonian. The difference of the dynamics results between model system and realistic system suggests that it is necessary to perform the on-the-fly dynamics to study the complex molecular system in some cases. Overall, considering the excellent performance of the SQC/MM method in this work, it provides us with a powerful tool to study the ISC process in the future, in both the model and realistic systems.

■ ASSOCIATED CONTENT

Supporting Information

The Supporting Information is available free of charge at https://pubs.acs.org/doi/10.1021/acs.jctc.5c00397.

Details of the implementation ISC dynamics in the TSH method; brief introduction to the ML-MCTDH method and the related computational details; parameters used in the model Hamiltonian; number of trajectories inside/outside the window in the SQC/MM dynamics; and trajectory convergence tests for the model system dynamics with the TSH and SQC/MM methods (PDF)

■ AUTHOR INFORMATION

Corresponding Authors

Deping Hu − *Department of Chemistry, Faculty of Arts and Sciences, Center for Advanced Materials Research, Beijing Normal University, Zhuhai 519087, China;* orcid.org/0000-0001-7161-1253; Email: deping.hu@bnu.edu.cn

https://doi.org/10.1021/acs.jctc.5c00397
J. Chem. Theory Comput. 2025, 21, 4386−4396

Ya-Jun Liu − *Department of Chemistry, Faculty of Arts and Sciences, Center for Advanced Materials Research, Beijing Normal University, Zhuhai 519087, China; Key Laboratory of Theoretical and Computational Photochemistry, Ministry of Education, College of Chemistry, Beijing Normal University, Beijing 100875, China;* orcid.org/0000-0001-8761-5339; Email: yajun.liu@bnu.edu.cn

Authors

Haiyi Huang − *Department of Chemistry, Faculty of Arts and Sciences, Center for Advanced Materials Research, Beijing Normal University, Zhuhai 519087, China*

Jiawei Peng − *SCNU Environmental Research Institute, Guangdong Provincial Key Laboratory of Chemical Pollution and Environmental Safety & MOE Key Laboratory of Environmental Theoretical Chemistry, School of Environment, South China Normal University, Guangzhou 510006, China*

Zhenggang Lan − *SCNU Environmental Research Institute, Guangdong Provincial Key Laboratory of Chemical Pollution and Environmental Safety & MOE Key Laboratory of Environmental Theoretical Chemistry, School of Environment, South China Normal University, Guangzhou 510006, China;* orcid.org/0000-0002-8509-0388

Complete contact information is available at: https://pubs.acs.org/10.1021/acs.jctc.5c00397

Notes

The authors declare no competing financial interest.

■ ACKNOWLEDGMENTS

This work was supported by grants from the National Natural Science Foundation of China (Grant Nos. 22403008, 22373010, 21973005, 22333003 and 22361132528), the Beijing Natural Science Foundation (Grant No. 2244074), the Guangdong Basic and Applied Basic Research Foundation (Grant No. 2025A1515012183), and the start-up funding from Beijing Normal University (Grant No. 312200502511). Computing resources were provided by the Interdisciplinary Intelligence Super Computer Center of Beijing Normal University at Zhuhai. We gratefully acknowledge HZWTECH for providing computation facilities.

■ REFERENCES

(1) Domcke, W.; Koppel, H.; Yarkony, D. R. *Conical Intersections: Electronic Structure, Dynamics & Spectroscopy*; World Scientific, 2004; Vol. *15*.

(2) Domcke, W.; Yarkony, D. *Conical Intersections: Theory, Computation and Experiment*; World Scientific, 2011; Vol. *17*.

(3) Kumpulainen, T.; Lang, B.; Rosspeintner, A.; Vauthey, E. Ultrafast Elementary Photochemical Processes of Organic Molecules in Liquid Solution. *Chem. Rev.* **2017**, *117*, 10826−10939.

(4) Domcke, W.; Yarkony, D. R. Role of Conical Intersections in Molecular Spectroscopy and Photoinduced Chemical Dynamics. *Annu. Rev. Phys. Chem.* **2012**, *63*, 325−352.

(5) Penfold, T. J.; Gindensperger, E.; Daniel, C.; Marian, C. M. Spin-Vibronic Mechanism for Intersystem Crossing. *Chem. Rev.* **2018**, *118*, 6975−7025.

(6) Eng, J.; Gourlaouen, C.; Gindensperger, E.; Daniel, C. Spin-Vibronic Quantum Dynamics for Ultrafast Excited-State Processes. *Acc. Chem. Res.* **2015**, *48*, 809−817.

(7) Šrut, A.; Mai, S.; Sazanovich, I. V.; Heyda, J.; Vlček, A.; González, L.; Záliš, S. Nonadiabatic excited-state dynamics of $ReCl(CO)_3(bpy)$ in two different solvents. *Phys. Chem. Chem. Phys.* **2022**, *24*, 25864−25877.

(8) Capano, G.; Chergui, M.; Rothlisberger, U.; Tavernelli, I.; Penfold, T. J. A Quantum Dynamics Study of the Ultrafast Relaxation in a Prototypical Cu(I)−Phenanthroline. *J. Phys. Chem. A* **2014**, *118*, 9861−9869.

(9) Gibson, J.; Monkman, A. P.; Penfold, T. J. The Importance of Vibronic Coupling for Efficient Reverse Intersystem Crossing in Thermally Activated Delayed Fluorescence Molecules. *ChemPhysChem* **2016**, *17*, 2956−2961.

(10) Uoyama, H.; Goushi, K.; Shizu, K.; Nomura, H.; Adachi, C. Highly efficient organic light-emitting diodes from delayed fluorescence. *Nature* **2012**, *492*, 234−238.

(11) Peng, Q.; Niu, Y.; Shi, Q.; Gao, X.; Shuai, Z. Correlation Function Formalism for Triplet Excited State Decay: Combined Spin−Orbit and Nonadiabatic Couplings. *J. Chem. Theory Comput.* **2013**, *9*, 1132−1143.

(12) Vacher, M.; Fdez Galván, I.; Ding, B.-W.; Schramm, S.; Berraud-Pache, R.; Naumov, P.; Ferré, N.; Liu, Y.-J.; Navizet, I.; Roca-Sanjuán, D.; Baader, W. J.; Lindh, R. Chemi- and Bioluminescence of Cyclic Peroxides. *Chem. Rev.* **2018**, *118*, 6927−6974.

(13) Liu, Y.-J. Understanding the complete bioluminescence cycle from a multiscale computational perspective: A review. *J. Photochem. Photobiol. C: Photochem. Rev.* **2022**, *52*, No. 100537.

(14) Crespo-Otero, R.; Barbatti, M. Recent Advances and Perspectives on Nonadiabatic Mixed Quantum−Classical Dynamics. *Chem. Rev.* **2018**, *118*, 7026−7068.

(15) Franco de Carvalho, F.; Tavernelli, I. Nonadiabatic dynamics with intersystem crossings: A time-dependent density functional theory implementation. *J. Chem. Phys.* **2015**, *143*, No. 224105.

(16) Granucci, G.; Persico, M.; Spighi, G. Surface hopping trajectory simulations with spin-orbit and dynamical couplings. *J. Chem. Phys.* **2012**, *137*, No. 22A501.

(17) Richter, M.; Marquetand, P.; González-Vázquez, J.; Sola, I.; González, L. SHARC: ab Initio Molecular Dynamics with Surface Hopping in the Adiabatic Representation Including Arbitrary Couplings. *J. Chem. Theory Comput.* **2011**, *7*, 1253−1258.

(18) Fay, T. P.; Manolopoulos, D. E. Radical pair intersystem crossing: Quantum dynamics or incoherent kinetics? *J. Chem. Phys.* **2019**, *150*, No. 151102.

(19) Fedorov, D. A.; Pruitt, S. R.; Keipert, K.; Gordon, M. S.; Varganov, S. A. Ab Initio Multiple Spawning Method for Intersystem Crossing Dynamics: Spin-Forbidden Transitions between 3B1 and 1A1 States of GeH2. *J. Phys. Chem. A* **2016**, *120*, 2911−2919.

(20) Beck, M.; Jäckle, A.; Worth, G.; Meyer, H.-D. The multiconfiguration time-dependent Hartree (MCTDH) method: a highly efficient algorithm for propagating wavepackets. *Phys. Rep.* **2000**, *324*, 1−105.

(21) Tanimura, Y. Nonperturbative expansion method for a quantum system coupled to a harmonic-oscillator bath. *Phys. Rev. A* **1990**, *41*, 6676−6687.

(22) Tanimura, Y. Stochastic Liouville, Langevin, Fokker−Planck, and Master Equation Approaches to Quantum Dissipative Systems. *J. Phys. Soc. Jpn.* **2006**, *75*, No. 082001.

(23) Wang, L.; Akimov, A.; Prezhdo, O. V. Recent Progress in Surface Hopping: 2011−2015. *J. Phys. Chem. Lett.* **2016**, *7*, 2100−2112.

(24) Tully, J. C. Molecular dynamics with electronic transitions. *J. Chem. Phys.* **1990**, *93*, 1061−1071.

(25) Mai, S.; Marquetand, P.; González, L. A general method to describe intersystem crossing dynamics in trajectory surface hopping. *Int. J. Quantum Chem.* **2015**, *115*, 1215−1231.

(26) Cui, G.; Thiel, W. Generalized trajectory surface-hopping method for internal conversion and intersystem crossing. *J. Chem. Phys.* **2014**, *141*, No. 124101.

(27) Xu, C.; Gu, F. L.; Zhu, C. Ultrafast intersystem crossing for nitrophenols: ab initio nonadiabatic molecular dynamics simulation. *Phys. Chem. Chem. Phys.* **2018**, *20*, 5606−5616.

(28) Yue, L.; Yu, L.; Xu, C.; Zhu, C.; Liu, Y. Quantum yields of singlet and triplet chemiexcitation of dimethyl 1,2-dioxetane: ab initio nonadiabatic molecular dynamic simulations. *Phys. Chem. Chem. Phys.* **2020**, *22*, 11440−11451.
(29) Mai, S.; Marquetand, P.; González, L. Nonadiabatic dynamics: The SHARC approach. *WIREs Comput. Mol. Sci.* **2018**, *8*, No. e1370.
(30) Wada, S.; Tsutsumi, T.; Saita, K.; Taketsugu, T. Ab initio molecular dynamics study of intersystem crossing dynamics for MH (M = Si, Ge, Sn, Pb) on spin-pure and spin-mixed potential energy surfaces. *J. Comput. Chem.* **2024**, *45*, 552−562.
(31) Subotnik, J. E.; Jain, A.; Landry, B.; Petit, A.; Ouyang, W.; Bellonzi, N. Understanding the Surface Hopping View of Electronic Transitions and Decoherence. *Annu. Rev. Phys. Chem.* **2016**, *67*, 387−417.
(32) Meyera, H.-D.; Miller, W. H. A classical analog for electronic degrees of freedom in nonadiabatic collision processes. *J. Chem. Phys.* **1979**, *70*, 3214−3223.
(33) Cotton, S. J.; Miller, W. H. Symmetrical windowing for quantum states in quasi-classical trajectory simulations: Application to electronically non-adiabatic processes. *J. Chem. Phys.* **2013**, *139*, No. 234112.
(34) Cotton, S. J.; Miller, W. H. Symmetrical Windowing for Quantum States in Quasi-Classical Trajectory Simulations. *J. Phys. Chem. A* **2013**, *117*, 7190−7194.
(35) Cotton, S. J.; Miller, W. H. The Symmetrical Quasi-Classical Model for Electronically Non-Adiabatic Processes Applied to Energy Transfer Dynamics in Site-Exciton Models of Light-Harvesting Complexes. *J. Chem. Theory Comput.* **2016**, *12*, 983−991.
(36) Cotton, S. J.; Miller, W. H. A new symmetrical quasi-classical model for electronically non-adiabatic processes: Application to the case of weak non-adiabatic coupling. *J. Chem. Phys.* **2016**, *145*, No. 144108.
(37) Cotton, S. J.; Miller, W. H. A symmetrical quasi-classical windowing model for the molecular dynamics treatment of non-adiabatic processes involving many electronic states. *J. Chem. Phys.* **2019**, *150*, No. 104101.
(38) Cotton, S. J.; Miller, W. H. Trajectory-adjusted electronic zero point energy in classical Meyer-Miller vibronic dynamics: Symmetrical quasiclassical application to photodissociation. *J. Chem. Phys.* **2019**, *150*, No. 194110.
(39) Miller, W. H.; Cotton, S. J. Classical molecular dynamics simulation of electronically non-adiabatic processes. *Faraday Discuss.* **2016**, *195*, 9−30.
(40) Kananenka, A. A.; Hsieh, C.-Y.; Cao, J.; Geva, E. Nonadiabatic Dynamics via the Symmetrical Quasi-Classical Method in the Presence of Anharmonicity. *J. Phys. Chem. Lett.* **2018**, *9*, 319−326.
(41) Liang, R.; Cotton, S. J.; Binder, R.; Hegger, R.; Burghardt, I.; Miller, W. H. The symmetrical quasi-classical approach to electronically nonadiabatic dynamics applied to ultrafast exciton migration processes in semiconducting polymers. *J. Chem. Phys.* **2018**, *149*, 044101 DOI: 10.1063/1.5037815.
(42) Provazza, J.; Coker, D. F. Communication: Symmetrical quasi-classical analysis of linear optical spectroscopy. *J. Chem. Phys.* **2018**, *148*, 181102 DOI: 10.1063/1.5031788.
(43) Zheng, J.; Xie, Y.; Jiang, S.-s.; Long, Y.-z.; Ning, X.; Lan, Z.-g. Ultrafast Electron Transfer with Symmetrical Quasi-classical Dynamics based on Mapping Hamiltonian and Quantum Dynamics based on ML-MCTDH†. *Chin. J. Chem. Phys.* **2017**, *30*, 800−810.
(44) Hu, D.; Xie, Y.; Peng, J.; Lan, Z. On-the-Fly Symmetrical Quasi-Classical Dynamics with Meyer-Miller Mapping Hamiltonian for the Treatment of Nonadiabatic Dynamics at Conical Intersections. *J. Chem. Theory Comput.* **2021**, *17*, 3267−3279.
(45) Xie, Y.; Zheng, J.; Lan, Z. Performance evaluation of the symmetrical quasi-classical dynamics method based on Meyer-Miller mapping Hamiltonian in the treatment of site-exciton models. *J. Chem. Phys.* **2018**, *149*, No. 174105.
(46) Zheng, J.; Peng, J.; Xie, Y.; Long, Y.; Ning, X.; Lan, Z. Study of the exciton dynamics in perylene bisimide (PBI) aggregates with symmetrical quasiclassical dynamics based on the Meyer−Miller mapping Hamiltonian. *Phys. Chem. Chem. Phys.* **2020**, *22*, 18192−18204.
(47) Gao, X.; Saller, M. A. C.; Liu, Y.; Kelly, A.; Richardson, J. O.; Geva, E. Benchmarking Quasiclassical Mapping Hamiltonian Methods for Simulating Electronically Nonadiabatic Molecular Dynamics. *J. Chem. Theory Comput.* **2020**, *16*, 2883−2895.
(48) Tao, G. Understanding Electronically Non-Adiabatic Relaxation Dynamics in Singlet Fission. *J. Chem. Theory Comput.* **2015**, *11*, 28−36.
(49) Zhou, W.; Mandal, A.; Huo, P. Quasi-Diabatic Scheme for Nonadiabatic On-the-Fly Simulations. *J. Phys. Chem. Lett.* **2019**, *10*, 7062−7070.
(50) Hu, D.; Mandal, A.; Weight, B. M.; Huo, P. Quasi-diabatic propagation scheme for simulating polariton chemistry. *J. Chem. Phys.* **2022**, *157*, No. 194109.
(51) Hu, D.; Ying, W.; Huo, P. Resonance Enhancement of Vibrational Polariton Chemistry Obtained from the Mixed Quantum-Classical Dynamics Simulations. *J. Phys. Chem. Lett.* **2023**, *14*, 11208−11216.
(52) Talbot, J. J.; Head-Gordon, M.; Cotton, S. J. The symmetric quasi-classical model using on-the-fly time-dependent density functional theory within the Tamm-Dancoff approximation. *Mol. Phys.* **2023**, *121*, No. e2153761.
(53) He, X.; Cheng, X.; Wu, B.; Liu, J. Nonadiabatic Field with Triangle Window Functions on Quantum Phase Space. *J. Phys. Chem. Lett.* **2024**, *15*, 5452−5466.
(54) Tang, D.; Fang, W.-H.; Shen, L.; Cui, G. Combining Meyer-Miller Hamiltonian with electronic structure methods for on-the-fly nonadiabatic dynamics simulations: implementation and application. *Phys. Chem. Chem. Phys.* **2019**, *21*, 17109−17117.
(55) Hu, Z.; Sun, X. All-Atom Nonadiabatic Semiclassical Mapping Dynamics for Photoinduced Charge Transfer of Organic Photovoltaic Molecules in Explicit Solvents. *J. Chem. Theory Comput.* **2022**, *18*, 5819−5836.
(56) Weight, B. M.; Mandal, A.; Huo, P. Ab initio symmetric quasi-classical approach to investigate molecular Tully models. *J. Chem. Phys.* **2021**, *155*, No. 084106.
(57) Du, L.; Lan, Z. An On-the-Fly Surface-Hopping Program JADE for Nonadiabatic Molecular Dynamics of Polyatomic Systems: Implementation and Applications. *J. Chem. Theory Comput.* **2015**, *11*, 1360−1374.
(58) Cannizzo, A.; Blanco-Rodríguez, A. M.; El Nahhas, A.; Šebera, J.; Záliš, S.; Vlček, A. J.; Chergui, M. Femtosecond Fluorescence and Intersystem Crossing in Rhenium(I) Carbonyl−Bipyridine Complexes. *J. Am. Chem. Soc.* **2008**, *130*, 8967−8974.
(59) Müller, U.; Stock, G. Flow of zero-point energy and exploration of phase space in classical simulations of quantum relaxation dynamics. II. Application to nonadiabatic processes. *J. Chem. Phys.* **1999**, *111*, 77−88.
(60) Runeson, J. E.; Richardson, J. O. Spin-mapping approach for nonadiabatic molecular dynamics. *J. Chem. Phys.* **2019**, *151*, No. 044119.
(61) Runeson, J. E.; Richardson, J. O. Generalized spin mapping for quantum-classical dynamics. *J. Chem. Phys.* **2020**, *152*, No. 084110.
(62) Mandal, A.; Shakib, F. A.; Huo, P. Investigating photoinduced proton coupled electron transfer reaction using quasi diabatic dynamics propagation. *J. Chem. Phys.* **2018**, *148*, No. 244102.
(63) Mandal, A.; Sandoval C, J. S.; Shakib, F. A.; Huo, P. Quasi-Diabatic Propagation Scheme for Direct Simulation of Proton-Coupled Electron Transfer Reaction. *J. Phys. Chem. A* **2019**, *123*, 2470−2482.
(64) Meyer, H.-D.; Worth, G. A. Quantum molecular dynamics: propagating wavepackets and density operators using the multi-configuration time-dependent Hartree method. *Theor. Chem. Acc.* **2003**, *109*, 251−267.
(65) Vendrell, O.; Meyer, H.-D. Multilayer multiconfiguration time-dependent Hartree method: Implementation and applications to a Henon−Heiles Hamiltonian and to pyrazine. *J. Chem. Phys.* **2011**, *134*, No. 044135.

(66) Perdew, J. P.; Burke, K.; Ernzerhof, M. Generalized Gradient Approximation Made Simple. *Phys. Rev. Lett.* **1996**, *77*, 3865−3868.
(67) Adamo, C.; Barone, V. Toward reliable density functional methods without adjustable parameters: The PBE0 model. *J. Chem. Phys.* **1999**, *110*, 6158−6170.
(68) Hay, P. J.; Wadt, W. R. Ab initio effective core potentials for molecular calculations. Potentials for K to Au including the outermost core orbitals. *J. Chem. Phys.* **1985**, *82*, 299−310.
(69) Hehre, W. J.; Ditchfield, R.; Pople, J. A. SelfConsistent Molecular Orbital Methods. XII. Further Extensions of GaussianType Basis Sets for Use in Molecular Orbital Studies of Organic Molecules. *J. Chem. Phys.* **1972**, *56*, 2257−2261.
(70) Grimme, S. Semiempirical GGA-type density functional constructed with a long-range dispersion correction. *J. Comput. Chem.* **2006**, *27*, 1787−1799.
(71) Barone, V.; Cossi, M. Quantum Calculation of Molecular Energies and Energy Gradients in Solution by a Conductor Solvent Model. *J. Phys. Chem. A* **1998**, *102*, 1995−2001.
(72) Cossi, M.; Rega, N.; Scalmani, G.; Barone, V. Energies, structures, and electronic properties of molecules in solution with the C-PCM solvation model. *J. Comput. Chem.* **2003**, *24*, 669−681.
(73) Frisch, M. J.; Trucks, G. W.; Schlegel, H. B.; Scuseria, G. E.; Robb, M. A.; Cheeseman, J. R.; Scalmani, G.; Barone, V.; Petersson, G. A.; Nakatsuji, H.; Li, X.; Caricato, M.; Marenich, A. V.; Bloino, J.; Janesko, B. G.; Gomperts, R.; Mennucci, B.; Hratchian, H. P.; Ortiz, J. V.; Izmaylov, A. F.; Sonnenberg, J. L.; Williams-Young, D.; Ding, F.; Lipparini, F.; Egidi, F.; Goings, J.; Peng, B.; Petrone, A.; Henderson, T.; Ranasinghe, D.; Zakrzewski, V. G.; Gao, J.; Rega, N.; Zheng, G.; Liang, W.; Hada, M.; Ehara, M.; Toyota, K.; Fukuda, R.; Hasegawa, J.; Ishida, M.; Nakajima, T.; Honda, Y.; Kitao, O.; Nakai, H.; Vreven, T.; Throssell, K.; Montgomery, J. A., Jr.; Peralta, J. E.; Ogliaro, F.; Bearpark, M. J.; Heyd, J. J.; Brothers, E. N.; Kudin, K. N.; Staroverov, V. N.; Keith, T. A.; Kobayashi, R.; Normand, J.; Raghavachari, K.; Rendell, A. P.; Burant, J. C.; Iyengar, S. S.; Tomasi, J.; Cossi, M.; Millam, J. M.; Klene, M.; Adamo, C.; Cammi, R.; Ochterski, J. W.; Martin, R. L.; Morokuma, K.; Farkas, O.; Foresman, J. B.; Fox, D. J. *Gaussian Inc 16. Revision B.01*; Gaussian Inc.: Wallingford CT, 2016.
(74) Wigner, E. On the Quantum Correction For Thermodynamic Equilibrium. *Phys. Rev.* **1932**, *40*, 749−759.
(75) Shao, Y.; Gan, Z.; Epifanovsky, E.; Gilbert, A. T.; Wormit, M.; Kussmann, J.; Lange, A. W.; Behn, A.; Deng, J.; Feng, X.; et al. Advances in molecular quantum chemistry contained in the Q-Chem 4 program package. *Mol. Phys.* **2015**, *113*, 184−215.

https://doi.org/10.1021/acs.jctc.5c00397
J. Chem. Theory Comput. 2025, 21, 4386−4396